Urban green space and peri-urban forest microclimates in the city of Augsburg, Germany: a seasonal and synoptic perspective

Jonathan Simon, Max Stocker, Lisa-Marie Falkenrodt, Bhargavi Mahesh, Joachim Rathmann, Wolfgang Buermann, Yekta Said Can, Elisabeth André, Christoph Beck

Angaben zur Veröffentlichung / Publication details:

Simon, Jonathan, Max Stocker, Lisa-Marie Falkenrodt, Bhargavi Mahesh, Joachim Rathmann, Wolfgang Buermann, Yekta Said Can, Elisabeth André, and Christoph Beck. 2026. "Urban green space and peri-urban forest microclimates in the city of Augsburg, Germany: a seasonal and synoptic perspective." *Urban Forestry & Urban Greening* 124: 129617. https://doi.org/10.1016/j.ufug.2026.129617.

Urban Forestry & Urban Greening 124 (2026) 129617

Contents lists available at ScienceDirect

Urban Forestry & Urban Greening

journal homepage: www.elsevier.com/locate/ufug

Original article

Urban green space and peri-urban forest microclimates in the city of Augsburg, Germany: A seasonal and synoptic perspective

Jonathan Simon [a,*], Max Stocker [a], Lisa-Marie Falkenrodt [a], Bhargavi Mahesh [b], Joachim Rathmann [a], Wolfgang Buermann [a,c], Yekta Said Can [b], Elisabeth André [b], Christoph Beck [a,c]

[a] *Chair of Physical Geography and Climate Science, Institute of Geography, University of Augsburg, Alter Postweg 118, Augsburg D - 86159, Germany*
[b] *Chair of Human-Centered Artificial Intelligence, Institute of Computer Science, University of Augsburg, Universitätsstraße 6a, Augsburg D - 86159, Germany*
[c] *Centre for Climate Resilience - CCR, University of Augsburg, Universitätsstraße 12, Augsburg D - 86159, Germany*

A B S T R A C T

Urban green spaces (UGS), including peri-urban forests, are recognised as effective climate adaptation measures. However, research into the microclimate characteristics of different UGS structures under varying diurnal, seasonal and synoptic conditions is scarce. Over two annual cycles, this study collected climate data from five structurally diverse UGS and one vegetated residential district across Augsburg, Germany. The UGS covered mixed forests, pine forest, heathland, and an urban park. Results show that diurnal air temperature contrasts exceeded seasonal and synoptic variability across all sites. Mixed forests exhibited the largest daytime cooling capacity and the least diurnal temperature variability. Although the urban park exhibited higher cooling capacity than the pine forest and heathland at noon, its nighttime cooling effect relative to the peri-urban forests was modest. Air temperature differences between the UGS structures increased with warmer weather and vice versa. Large-scale weather conditions either dampened temperature contrasts under cool, windy and overcast situations or amplified them during calm, clear-sky conditions. Mixed-effects modelling indicated that tree density had the strongest overall association with lower air temperatures, particularly at night. In contrast, tree height was linked to moderate daytime cooling but consistent nighttime warming, presumably due to reduced longwave radiative losses. During a heatwave event, mixed forests reduced maximum Modified Physiologically Equivalent Temperature by around 6 °C. These findings inform heat action planning by showing that the UGS cooling efficiency depends on weather conditions and time of day, and that structurally diverse mixed peri-urban forests reduce heat stress most effectively.

1. Introduction

Cities are the economic and social hubs of the modern world, providing opportunities for innovation, education, health services, security, and social life (Ulgiati and Zucaro, 2019). However, urbanisation also amplifies exposure to climate and environmental hazards (Dodman et al., 2022), including flooding (Cea and Costabile, 2022), air pollution (Sicard et al., 2023), and biodiversity loss (Elmqvist et al., 2013). The urban heat island (UHI) effect refers to the phenomenon in which urban areas exhibit higher air temperatures (T_a) than surrounding rural areas due to the predominance of impervious surfaces, reduced vegetation, and anthropogenic heat emissions (Oke et al., 2017). Heatwaves amplify the UHI effect (Li and Bou-Zeid, 2013) and are expected to become more intense, more frequent, and longer-lasting in the future (Perkins-Kirkpatrick and Lewis, 2020). Extreme heat contributes to higher morbidity and mortality rates, particularly among vulnerable urban populations (Founda and Santamouris, 2017).

One of the most effective urban climate adaptation strategies is the implementation of green and blue infrastructures (Bowler et al., 2010; Gunawardena et al., 2017). While also vulnerable to climate change (Brandt et al., 2016), urban green spaces (UGS) provide valuable ecosystem services, including T_a, stormwater and air quality regulation, waste treatment, pollination, and recreation and aesthetic appreciation (Veerkamp et al., 2021). Urban parks, peri-urban forests, street trees, and vegetation on private land contribute to T_a reductions through evapotranspiration, shading, and increased surface roughness (Gunawardena et al., 2017). The cooling efficiency of UGS is influenced by multiple factors, including size and shape, vegetation type and diversity, canopy density, leaf area index, tree height, the presence of water bodies, and meteorological factors such as seasonality, sunlight

* Corresponding author.
E-mail addresses: jonathan.simon@uni-a.de (J. Simon), max.stocker@uni-a.de (M. Stocker), lisa-marie.falkenrodt@uni-a.de (L.-M. Falkenrodt), bhargavi.mahesh@uni-a.de (B. Mahesh), joachim.rathmann@uni-a.de (J. Rathmann), wolfgang.buermann@uni-a.de (W. Buermann), yekta.can@uni-a.de (Y.S. Can), elisabeth.andre@uni-a.de (E. André), christoph.beck@uni-a.de (C. Beck).

https://doi.org/10.1016/j.ufug.2026.129617
Received 9 March 2026; Received in revised form 30 May 2026; Accepted 3 July 2026
Available online 4 August 2026

exposure, and wind speed (Aram et al., 2019). While the positive effects of UGS are well studied, less attention has been given to how ecosystem services vary across different UGS structures – here defined by their structural tree compositions and usage properties. Focusing on T_a conditions, Arzberger et al. (2025) quantified the cooling effect of 36 urban parks in Munich, Germany, differing in size and vegetation complexity (encompassing vegetation structure, volume, density, and canopy cover). They found positive relationships between the UGS cooling effect and UGS size, as well as between the cooling effect and vegetation complexity. While their study focused on park-scale vegetation complexity quantified by mobile laser scanning, the present study compares structurally and functionally different UGS types under varying seasonal and synoptic conditions, thereby extending the analysis beyond park morphology alone.

Urban T_a varies with local site characteristics, local climate zones (LCZs), and prevailing synoptic conditions (Beck et al., 2018; Verdonck et al., 2018). While Beck et al. (2018) defined 16 synoptic categories based on local meteorological observations, large-scale weather types (Huth et al., 2008) are derived from gridded atmospheric datasets, such as pressure fields, and represent the combined effects of weather. Thus, associations between atmospheric circulation patterns and the regional surface environment can be examined (Yarnal, 1993). Previous research has primarily focused on links between large-scale atmospheric circulation and environmental hazards, including drought (Beck et al., 2015), heat (Adams et al., 2021), and extreme precipitation (Jacobeit et al., 2017), as well as to assess impacts on human health (Hondula et al., 2014; Simon et al., 2024). However, large-scale weather types are also particularly relevant in the context of UGS since they govern key atmospheric boundary conditions that control UGS cooling processes, including radiative forcing, wind-driven mixing and nocturnal atmospheric stability. To the best of our knowledge, however, no study to date has explicitly linked large-scale weather types to the microclimate

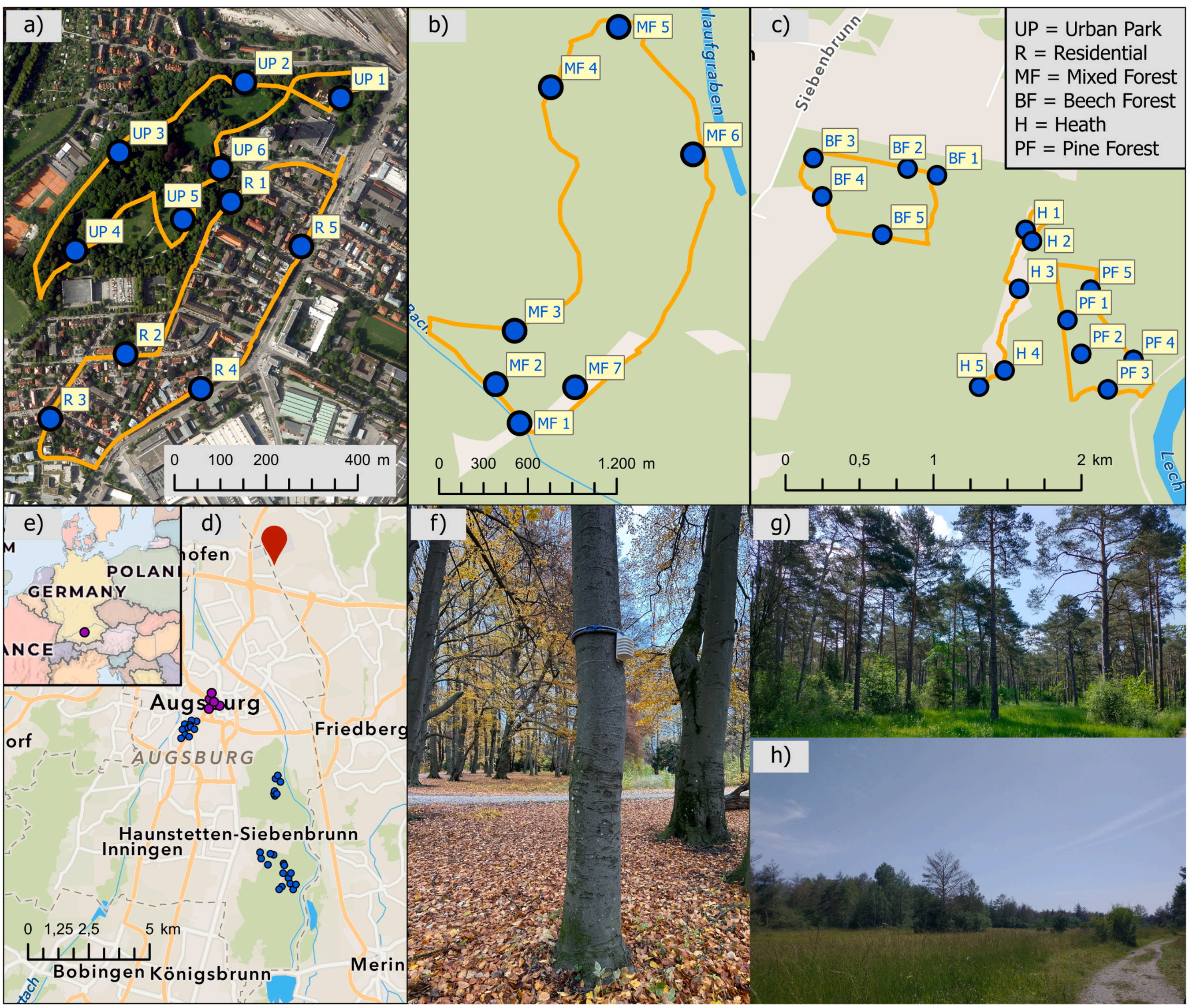

Fig. 1. UGS measurement network. The HOBO MX2301A logger locations (blue dots) for the five UGS and the residential site. The orange lines illustrate the routes on which mobile climate measurements were conducted during the summer of 2023. These measurements were used to establish the location of the logger sites (a–c; details are given in S1.1). Overview of the city of Augsburg, the UGS measurement network logger locations (blue dots), and the locations of five HOBO U23-001A loggers from the urban measurement network near the city centre (magenta dots). UP and R are the two sites near the city centre (blue dots). The peri-urban forest sites are located in the UFA southeast of the core city. The MF site is the northern site, while BF, H, and PF are situated in the southern district, in close proximity to each other. The nearest DWD station is indicated by a red sign (d). Overview map of Germany and the location of the measurement networks (e). The site UP 3. The logger is placed inside a self-constructed, 3D-printed radiation shield mounted on a tree (f). Visual impressions of the PF site and the H site during summer (g–h).

characteristics of various UGS structures.

Therefore, this study aims to quantify the impact of UGS structure on seasonal and diurnal T_a patterns, analyse how large-scale synoptic weather types influence these conditions, identify the main environmental drivers of T_a spatial variability, and evaluate human thermal comfort conditions in different UGS structures during extreme heat conditions.

2. Data and methods

2.1. Study areas

Six study sites representing structurally contrasting vegetated urban and peri-urban environments were investigated in Augsburg, a mid-sized city (approximately 301,000 citizens) in southern Bavaria, Germany (Fig. 1). Five sites represent distinct UGS structures, while one additional vegetated residential district (LCZ 5) was included as an urban reference site. The long-term annual mean T_a of Augsburg is 8.5 °C, with July being the warmest month at 18.1 °C. The city receives an average yearly precipitation of 767 mm, and the prevailing wind direction is southwest (Beck et al., 2018). The study sites encompass an 18 ha urban park (UP) – the Wittelsbacher Park – located within the western part of the city near the central railway station, a vegetated residential district (R) characterised by street trees and private gardens, and four more study sites within the urban forest of Augsburg (UFA): a mixed forest (MF), a mixed beech forest (BF), a pine forest (PF), and a heathland (H). These sites were selected to represent the dominant vegetated environments and vegetation structures present in Augsburg and its peri-urban surroundings. The selection therefore intentionally combines functional UGS types (urban park), forest compositions (mixed and pine forests), and open vegetation structures (heathland), reflecting the structural diversity of real-world urban and peri-urban green environments rather than a formal land-cover typology. As part of the interdisciplinary LEAF (Learning about the Effects of Augsburg Forest) project, site selection was additionally guided by accessibility, walkability, recreational relevance, and contrasting vegetation characteristics. Besides climatic analyses, the project investigated physiological and psychological responses to different urban forest environments. The residential district was included as a vegetated built-up comparison site to contextualise the cooling performance of the UGS structures relative to a typical low-density urban environment. Although not a UGS in the strict sense, the site is characterised by substantial vegetation cover and therefore represents an intermediate urban reference rather than a densely built urban core. Additional forest types, such as spruce or oak-dominated stands, were not included because they are uncommon in the Augsburg area.

2.2. Measurement networks

A measurement network comprising 33 MX2301A HOBO loggers from Onset (Onset, 2022) spread over all study sites (Fig. 1a–d) was established in late 2023. These loggers – placed inside self-constructed 3D-printed radiation shields (Fig. 1 f, Figure S7–S8) – measured T_a and relative humidity (RH) at 4-minute intervals. Depending on the UGS size, shape, and internal microclimatic heterogeneity identified during preliminary mobile climate measurements (see supplementary material S1.1), five to seven loggers were installed in each site to capture representative microclimatic conditions. Site-level analyses were based on aggregated measurements across all loggers within each UGS. The loggers were mounted on trees or lampposts at a height of 2.7 m to reduce vandalism risk. Before installation, sensitivity tests were conducted using two separate experimental setups: (1) climate and humidity chamber tests to evaluate the sensor accuracy (see S2.4.1) and (2) a field experiment at the rooftop of the University of Augsburg to assess the effects of different radiation shields (self-printed vs custom shields; see S2.4.2). A second, more urban-focused measurement network within the city of Augsburg still operates (Beck et al., 2018) and consists of HOBO U23–001A loggers (Onset, 2020). Loggers not representative of the UGS areas, e.g. R 1 (proximity to urban park), MF 7, and BF 4 (located at open meadows outside the forest), were excluded for site comparisons. Daily periods of positive (solar day) and negative (solar night) radiation balances (solar periods) were defined from one hour after sunrise to one hour before sunset (solar day) and from one hour after sunset to one hour before sunrise (solar night). The study period was set from January 2024 to December 2025, spanning two annual cycles to capture interannual variability and ensure robust assessments of seasonal and synoptic influences. Climate data from the nearest German Weather Service (DWD – Deutscher Wetterdienst) station, located northeast of Augsburg (Fig. 1d), complemented the data from the two measurement networks (DWD, 2026). More details on the study desgin and quality control of HOBO logger data are given in the supplementary material S1.1–S1.2.

2.3. Großwetter-types or prototype classification

This study employed the Großwetter-types (GWT) or prototype classification scheme (Beck et al., 2007, 2015) to classify the continuous atmosphere into distinct circulation classes. This method is based on predefined types, as initially defined by Hess and Brezowsky (1969). The primary objective is to characterise the circulation patterns in terms of varying degrees of zonality (Z), meridionality (M), and vorticity (V) of the large-scale pressure fields. The ten main circulation types are primarily defined by combining these three coefficients. Z and M define eight directional types depending on the main wind direction, and V determines the assignment of a central high or low-pressure type. A further refinement of the directional circulation types into cyclonic and anticyclonic subtypes based on the sign of V yields 18 types (Beck et al., 2007, 2015). GWTs were computed with the cost733class software version 1.4 (Philipp et al., 2010) using ERA5 reanalysis mean sea level pressure (MSLP) data on a 0.25° x 0.25° grid (Hersbach et al. 2023). GWTs were computed for a rectangular European spatial domain defined by the boundary coordinates 5° W – 25° E and 35° S – 61° N. To account for potential differences in synoptic forcing of day- and night-time UHI, GWTs were computed twice daily, based on MSLP fields at 12:00 UTC and 00:00 UTC. An illustration of all 18 GWTs is given in Figure S1.

2.4. Statistical analysis

The impact of seasonal, diurnal, and GWT effects on UGS T_a characteristics was investigated using a combination of exploratory (heatmaps, boxplots) and inferential statistical analyses. To test whether mean T_a values differed significantly across UGS sites, a one-way analysis of variance (ANOVA) followed by Tukey's Honest Significant Difference (HSD) was performed. When residuals were found to be non-normally distributed (Anderson-Darling test, $p \geq 0.05$), Kruskal-Wallis tests were conducted, followed by Dunn's multiple-comparison tests. These tests quantify the T_a difference between UGS and provide adjusted p-values that indicate the statistical significance of this difference. In order to identify the relative importance of local-environmental factors, linear mixed-effects models (LMMs) were fitted to daily T_a anomalies (relative to all loggers' mean T_a). Fixed effects included parameters and land-use types at the logger site, e.g., sky view factor (SVF), and within circular buffers with a radius of 150 m, such as number of trees or meadow areas (Table S2). This resulted in an additive model with three-way interactions between environmental fixed effects and season/solar period. Prior to modelling, numerical predictors were screened for high correlation. Pairs with Pearson's $r > 0.8$ were reduced to a single representative variable, and associations among categorical predictors were examined using Cramér's V. Variance inflation factors were computed to assess multicollinearity. Optimal model selection was based on the protocol outlined by Zuur et al. (2009), also put into practice and comprehensively documented by Oliveira et al. (2021). Effects were interpreted using marginal trends conditional on season and solar period. Data analysis was conducted in R (version 4.4.2) (R Core Team, 2024) utilising tidyverse packages (Wickham et al., 2019). LMMs were fitted using the lme function from the nlme package (Pinheiro et al., 2025). Tree and land use data were downloaded from LDBV (2024) and OpenStreetMap (2024). Normalized Difference Vegetation Index (NDVI) was derived from Sentinel Level 3 A data (German Aerospace Center, 2019). Seasonal SVF values were derived from hemispherical photographs (see S1.3) using the Sky-ViewFactorCalculator software (Lindberg and Holmer, 2024).

2.5. Approximation of thermal indices

To extend the assessment of near-surface T_a towards human-relevant thermal comfort conditions, a framework for approximating thermal indices was developed. This approach is demonstrated as a case study focusing on an heatwave event in August 2024. Thermal indices such as the Universal Thermal Climate Index (UTCI) (Bröde et al., 2012) and the Modified Physiologically Equivalent Temperature (mPET) (Chen and Matzarakis, 2018) are substantially more relevant to human well-being than T_a. These indices were computed using the Python (version 3.9.6) module *biometeo* (version 0.2.9) (Chen, 2023), a successor application of the RayMan software (Matzarakis et al., 2007, 2010). A central step in this workflow is the estimation of the mean radiant temperature (T_{MRT}). Site-specific input parameters included T_a, RH, longitude, latitude, elevation, SVF, environmental albedo (α_{env}), and the Bowen ratio (β). α_{env} was assigned according to LCZ following Stewart and Oke (2012), while β values were based on Christen and Vogt (2004). Additional variables required for T_{MRT} estimation – namely wind speed, cloud cover, and global and diffuse solar radiation – were obtained from the DWD station and used as proxies for all logger sites. Detailed workflows for the LMM setup and thermal index calculation are documented in the supplementary material S1.4–S1.5.

3. Results

3.1. Climatological and synoptical characterisation of the study period

First, the study period is analysed for its climatological and synoptic representativeness. The meteorological conditions for T_a and precipitation were found to largely fall within the long-term mean (Fig. 2). A total of 25 heat days ($T_{max} > 30$ °C) were recorded at the rural DWD station and 36 in the city centre according to the urban measurement network, indicating a pronounced UHI effect, particularly at night. While no tropical nights ($T_{min} > 20$ °C) occurred in the rural setting, 13 were observed within the city. Daily T_{min} frequently approached or exceeded the upper long-term range ($T_{mean} + 1\sigma$). May and September 2024 featured above-average amounts of precipitation, whereas the summer of 2025 was drier than usual. Synoptic conditions were also typical of the 30-year normal period from 1991 to 2020. Notably, there were few cyclonic GWTs alongside many high-pressure systems (> 1σ) during the summer months (see supplementary material S2.2 and Figure S2).

3.2. Seasonal and diurnal temperature variability

The study sites T_a characteristics varied more between solar day and solar night than between seasons, as evidenced by Fig. 3. Generally speaking, R and UP, MF and BF, and H and PF exhibited similar T_a characteristics. However, these characteristics were inconsistent across seasons and solar periods: R and UP differed during the solar day, with UP being cooler than R, particularly in the warmer seasons. H and PF, on the other hand, exhibited greater seasonal differences during the solar day, with larger T_a discrepancies observed in spring and winter. R was consistently the warmest site, with an average T_a anomaly of + 0.93 °C ± 0.38 °C relative to the mean of the study sites during the solar day, and + 1.48 °C ± 0.23 °C during the solar night, indicating a pronounced UHI effect despite the abundant vegetation present at this hybrid site. UP exhibited a cooling effect during the solar day, with a T_a anomaly of only + 0.11 °C ± 0.20 °C. However, during the solar night, UP was nearly as warm as R, with a T_a anomaly of + 1.06 °C ± 0.14 °C, indicating only a slight reduction in the UHI effect. MF and BF were the coolest sites during the day, with T_a anomalies of −0.81 °C ± 0.16 °C

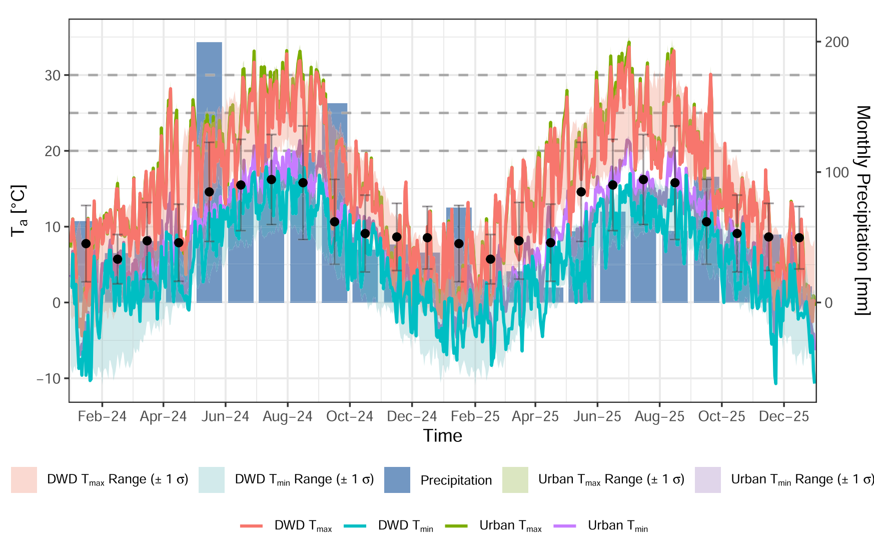

Fig. 2. General climatological characterisation of Augsburg for the study period. Daily maximum (DWD T_{max}) and minimum (DWD T_{min}) T_a as measured by the nearest station of the German Weather Service (DWD) and the urban climatological measurement network (Urban T_{max} and Urban T_{min}, respectively). The data from the urban network were aggregated from five HOBO U23-001A loggers located within and near Augsburg's city centre. Shaded areas represent the range, i.e., one standard deviation from the long-term daily means for the 30-year normal period from 1991 to 2020 for the DWD data, and one standard deviation across the five measurement values for the urban network. The bars in the background represent monthly amounts of precipitation, with the black dots and error bars indicating one standard deviation from monthly long-term means based on the normal period. Dashed lines indicate T_a thresholds for Tropical Nights (20 °C), Summer Days (25 °C) and Heat Days (30 °C), respectively.

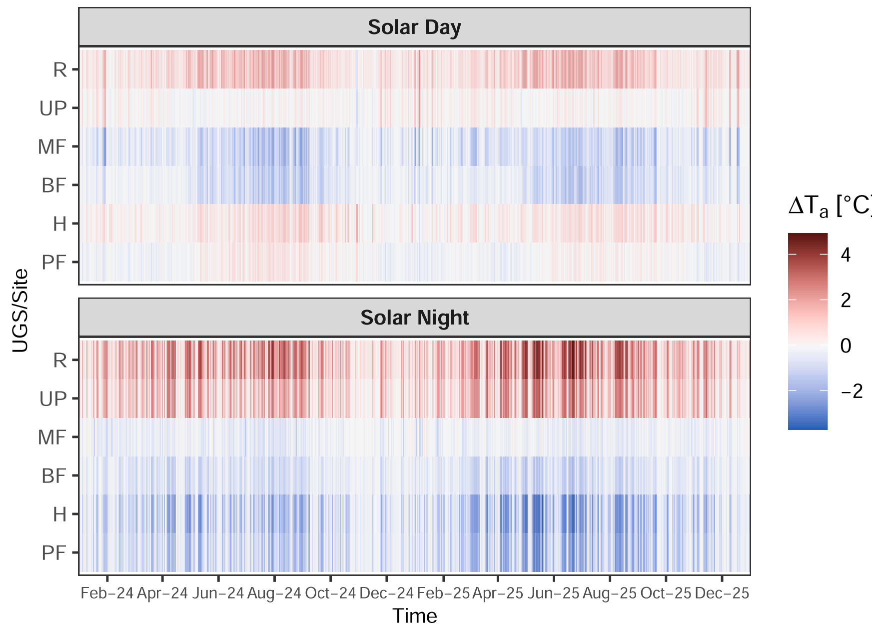

Fig. 3. T_a anomaly heatmap for the study period. Daily T_a anomalies relative to the averaged T_a of the six study sites during the study period, considering solar day and solar night.

and −0.66 °C ± 0.16 °C, respectively, highlighting the cooling potential of dense mixed peri-urban forests in a more rural setting. While the sparsely covered H and PF sites were, on average, warmer than the other sites during the day, with positive T_a anomalies of + 0.39 °C ± 0.33 °C (H) and + 0.05 °C ± 0.37 °C (PF) respectively, they were the coolest sites at night, with negative T_a anomalies of −1.05 °C ± 0.10 °C (H) and −0.92 °C ± 0.14 °C (PF) respectively. These results emphasise the importance of canopy coverage in controlling T_a variability.

To highlight T_a variability at seasonal levels and for extreme events such as summer days (SD), heat days (HD), freezing days (FD), and ice days (ID), Fig. 4 shows the study sites T_a anomalies aggregated to these levels. It proves that the differences between R and UP were primarily observed during the solar day, with the UP having the most potent cooling effect in spring and autumn, and the weakest effect in winter. During the solar day, MF and BF were the coolest sites throughout the year, with the most significant cooling effect observed in summer and during HD. During the solar night, on the other hand, H and PF were the coolest sites. While both sites were equally warm during summer (JJA) days, differences emerged in the other seasons, with PF being slightly cooler than the site average in spring (MAM) and winter (DJF). At the same time, H still showed positive T_a anomalies. The relative T_a site differences observed for the summer months, became even more pronounced for SD and HD, whereas they leveld off for FD and ID.

Next, we tested for significant differences in T_a characteristics among sites. Applying a one-way ANOVA to datasets covering each season and solar period separately yielded significant results ($p < 0.05$) for all eight models (four seasons × two solar periods). To study individual T_a differences, post-hoc comparisons were performed using Tukey's HSD test. Overall, 66% of pairwise comparisons were statistically significant ($p < 0.05$) (Fig. 5). These patterns were largely consistent across seasons, especially for the solar night. Solar day showed greater seasonal variability, with the smallest T_a differences during winter. The most significant T_a differences were found between R and H during solar nights. Generally, the strongest contrasts were observed between R/UP and the UFA sites, particularly during spring and summer.

Next, diurnal cycles of T_a anomalies across seasons and T_a events (HD, ID) were compared between the sites (Fig. 6). R was consistently the warmest site during the solar night, but T_a differences relative to H

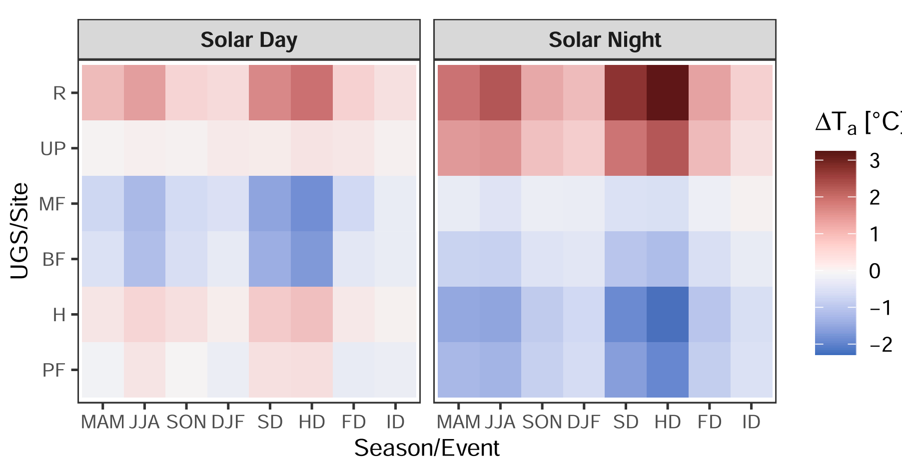

Fig. 4. T_a anomaly heatmap for seasons and special temperature events. T_a anomalies for spring (MAM), summer (JJA), autumn (SON), winter (DJF) and for the SD, HD, FD, and ID special temperature events during the study period, considering solar day and solar night. Anomalies were calculated at the seasonal/event level relative to the T_a of the six study sites.

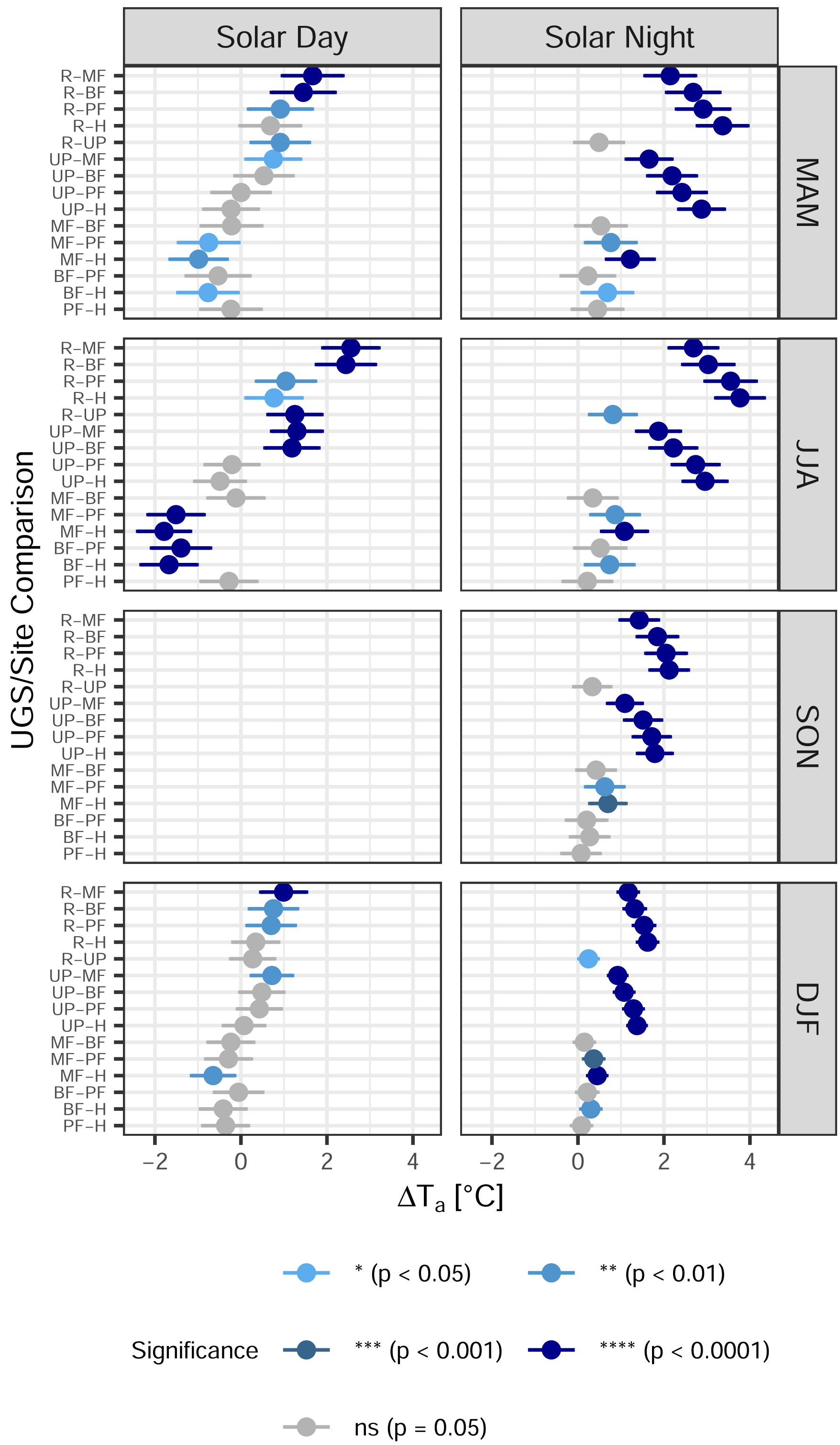

Fig. 5. Results of Tukey HSD post-hoc tests following significant ($p < 0.05$) one-way ANOVAs testing for differences in T_a among UGS structures/study sites, conducted separately for each season and for solar day and night. As residuals were not normally distributed for solar day in autumn (SON), ANOVA was not applied to this subset.

and PF decreased during the solar day, especially during summer, autumn and HD. On the other hand, H and PF were consistently the coolest UGS during the solar night. The boxplots revealed much greater T_a variability at H and PF than at the other sites. MF and BF featured the lowest T_a variability and were generally the coolest UGS during the day, especially during the summer and HD with strongest cooling effects during the morning and afternoon hours. Interestingly, these sub-daily cooling effects were also found for R, albeit weaker. UP showed greater T_a variability in spring and summer, with reduced variability in autumn and winter. R and DWD featured the lowest T_a variability across the seasons, i.e. diurnal cycles were most stable for these sites, whereas e.g. H and PF featured much greater T_a variability in the warm season

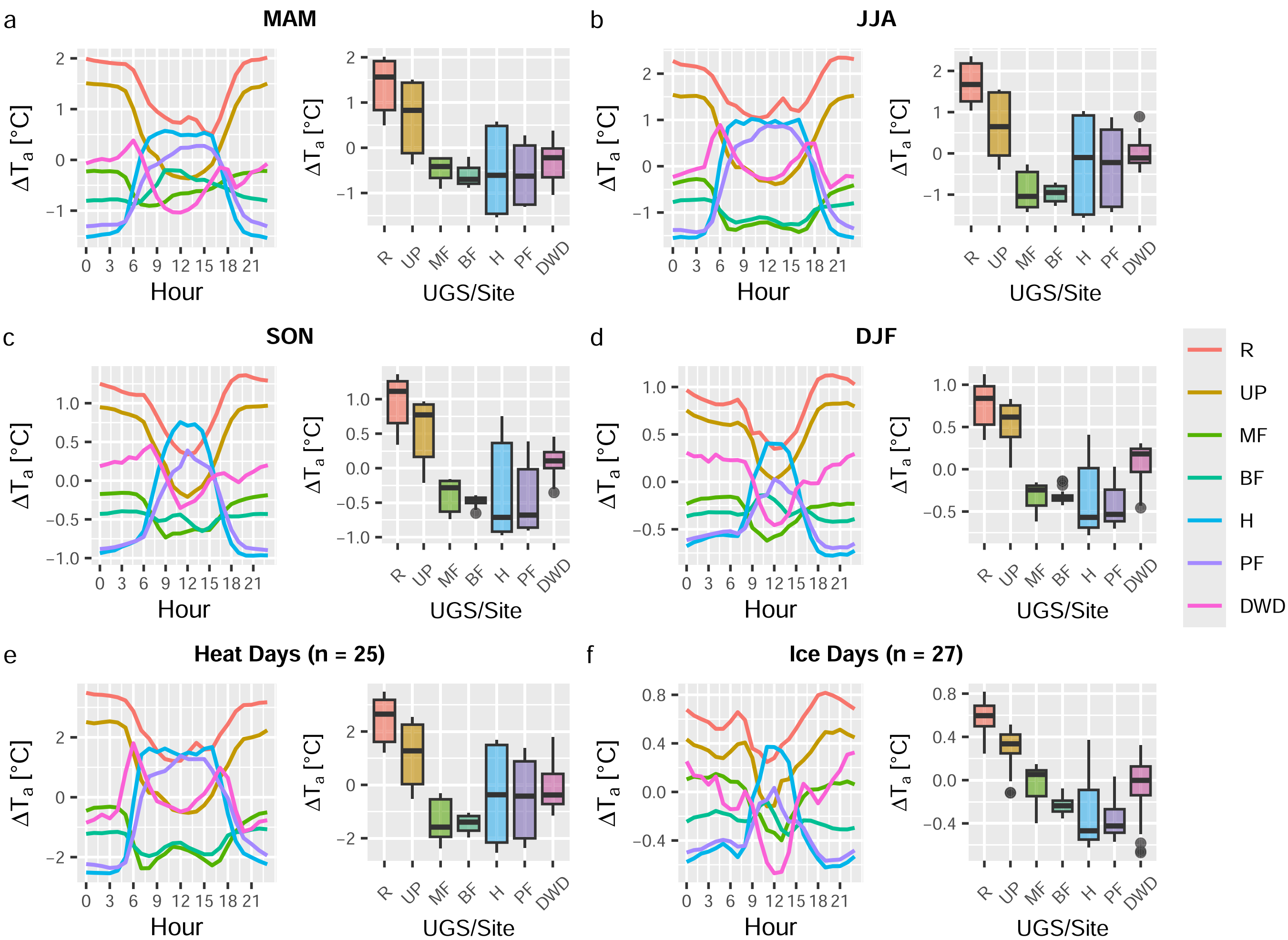

Fig. 6. Diurnal cycles of T_a anomalies (left panels) and corresponding boxplots summarising the distribution of hourly T_a anomalies (right panels) for each UGS/site across spring (MAM, a), summer (JJA, b), autumn (SON, c), and winter (DJF, d) as well as during heat days (HD, e) and ice days (ID, f). Lines represent mean hourly T_a anomalies for each site, while boxplots show the distribution of all hourly anomalies within the respective season or event. Colours consistently denote individual sites across line plots and boxplots. Anomalies were calculated relative to the mean T_a across the six study sites, excluding the DWD reference station.

than in the cold season.

3.3. Impact of GWTs

One of the primary motivations of our study was to investigate the effects of different large-scale weather types on UGS microclimates. The results showed that GWTs exerted distinct effects on T_a regimes across the study sites (Fig. 7). For example, T_a contrasts were more pronounced for anticyclonic than cyclonic GWTs. Southerly (SE-c, S-c, SW-ac) GWTs during the solar night featured positive T_a anomalies for R und UP and negative T_a anomalies for the UFA sites, especially H and PF. The differences during the solar night were minor for northerly GWTs. T_a differences between the sites were generally less pronounced for the solar day. However, easterly and southerly GWTs featured larger T_a site differences during both solar periods, with larger magnitudes during the solar day. Once again, minor T_a differences were evident in the northerly GWTs. The already established general T_a characteristics of the study sites (see Fig. 3) remained relatively constant under the influence of different GWTs, e.g. R and UP were always warmer during the solar night. However, GWTs modulated the intensity of these contrasts, as e.g. T_a differences tended to be weaker under northern types.

We further applied the statistical workflow described above (ANOVA followed by post hoc tests) separately for each GWT and solar period, resulting in 36 individual models (18 GWTs × 2 solar periods). Overall, T_a differences between study sites were more frequently significant during the solar night than during the solar day, and under anticyclonic rather than cyclonic conditions. Moreover, significant differences occurred predominantly under GWTs with northern, eastern or southern flow components, whereas westerly weather types generally exhibited weaker or non-significant contrasts. For instance, under a western cyclonic GWT during the solar night, significant T_a differences were limited to the urban–rural contrast, while other UGS comparisons were not significant. In contrast, nocturnal high-pressure situations produced significant T_a differences across most UGS types, indicating a strong amplification of microclimatic contrasts under calm and clear-sky conditions (Figures S3–S6).

3.4. Environmental drivers of temperature variability

To complement the UGS-type comparisons presented above, we applied LMMs to disentangle the relative influence of local environmental characteristics on T_a anomalies across all logger sites. In contrast to the preceding analyses, which focused on differences between predefined UGS categories, the mixed-effects approach shifts the perspective to the logger level and addresses the question of which structural and environmental factors drive T_a anomalies, how strongly they act, and how their effects vary with season and time of day. UGS structures are thus represented implicitly through their constituent characteristics (e.g., tree density, tree height, meadow areas, water surfaces), rather than as categorical units.

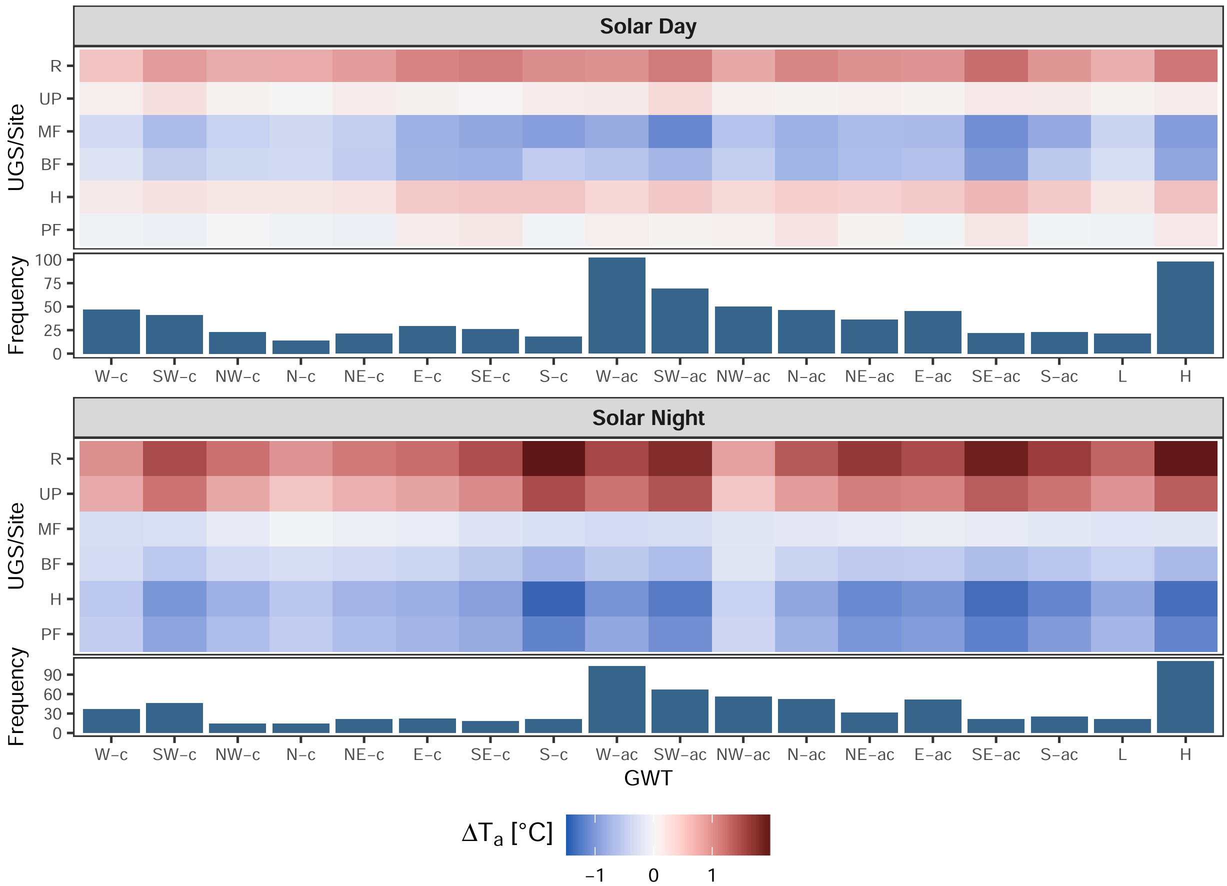

Fig. 7. GWT analysis. T_a anomalies for all GWTs for the six study sites during the study period, considering solar day and solar night (heatmap). Absolute frequencies of the GWTs for the solar day and the solar night (bar charts). Anomalies were calculated at the GWT level relative to the T_a of the six study sites. The GWT designations are shown on the x-axis. The uppercase letter(s) denote the main wind direction, whereas the lowercase letter(s) denote cyclonic (c) and anticyclonic (ac) subtypes. For instance, the GWT designated as SW-c is characterised by south-westerly winds and cyclonic dominance. L is a low-pressure system over Central Europe, while H is a high-pressure system over Central Europe.

Likelihood ratio tests following Zuur et al. (2009) indicated that all three-way interaction terms significantly improved model fit ($p < 0.01$). Only wind speed showed no significant main effect on T_a anomalies ($p = 0.88$). Random intercepts revealed moderate between-logger variability in mean T_a anomalies (SD = 0.16 °C), which was small compared to the residual within-logger variability (SD = 0.64 °C). The estimated autocorrelation parameter was close to zero (0.02), indicating negligible remaining serial dependence after accounting for fixed and random effects. Due to the extensive use of interaction terms, individual model coefficients are difficult to interpret directly. Therefore, effects were evaluated using marginal trends conditional on season and solar period (Fig. 8). Strong diurnal contrasts were evident across most predictors, whereas seasonal differences primarily modulated effect strength rather than direction. Number of trees, i.e. tree density, was consistently associated with lower T_a anomalies during both solar day and night, with markedly stronger cooling effects at night. Nighttime cooling intensified from winter to summer, reaching its largest magnitudes in spring and summer. Tree height showed weak or non-significant cooling during daytime but exhibited a consistent positive nighttime effect, indicating warmer nighttime conditions in areas with taller trees across all seasons. During the daytime, higher SVF was associated with greater T_a anomalies across all seasons, with effect sizes declining from summer to winter. At night, SVF effects were generally weak and negative in summer and spring, close to zero in autumn, and slightly positive in winter, indicating seasonally varying nocturnal radiative effects. NDVI effects were comparatively small. During the daytime, NDVI showed weak warming effects in autumn and cooling effects in spring and winter. In contrast, nighttime effects were small and inconsistent across seasons, suggesting that NDVI captured less relevant T_a variability than structural vegetation metrics. Land-use variables exhibited modest and predominantly nighttime effects. Meadow and heath areas were associated with reduced nighttime T_a anomalies across all seasons, with the strongest cooling observed in summer and spring. Daytime effects of these land-cover types were generally weak. Park and water areas showed only minor and ambiguous effects.

3.5. Case study: human thermal comfort conditions during a heatwave event

Extreme heat events put additional stress on trees because the demand for water is higher while its availability is lower due to higher rates of evapotranspiration. The resulting high vapour pressure deficits can lead to stomatal closure, reducing transpirational cooling. As a consequence, the cooling benefits of urban trees could decrease by up to 30% during heatwave events (Li et al., 2024). Assessing the cooling efficacy of UGS under such conditions is therefore critical to evaluating its effectiveness as a climate adaptation measure.

To address this, we analysed a multi-day heatwave event in August 2024, focusing not only on T_a but also on human thermal comfort (HTC) indices (UTCI and mPET), which better reflect heat stress experienced by urban residents. The heatwave analysis is presented descriptively; no additional statistical significance testing was performed for the thermal-index differences shown in Fig. 9. The large-scale atmospheric conditions during the heatwave event were characterised by high stability,

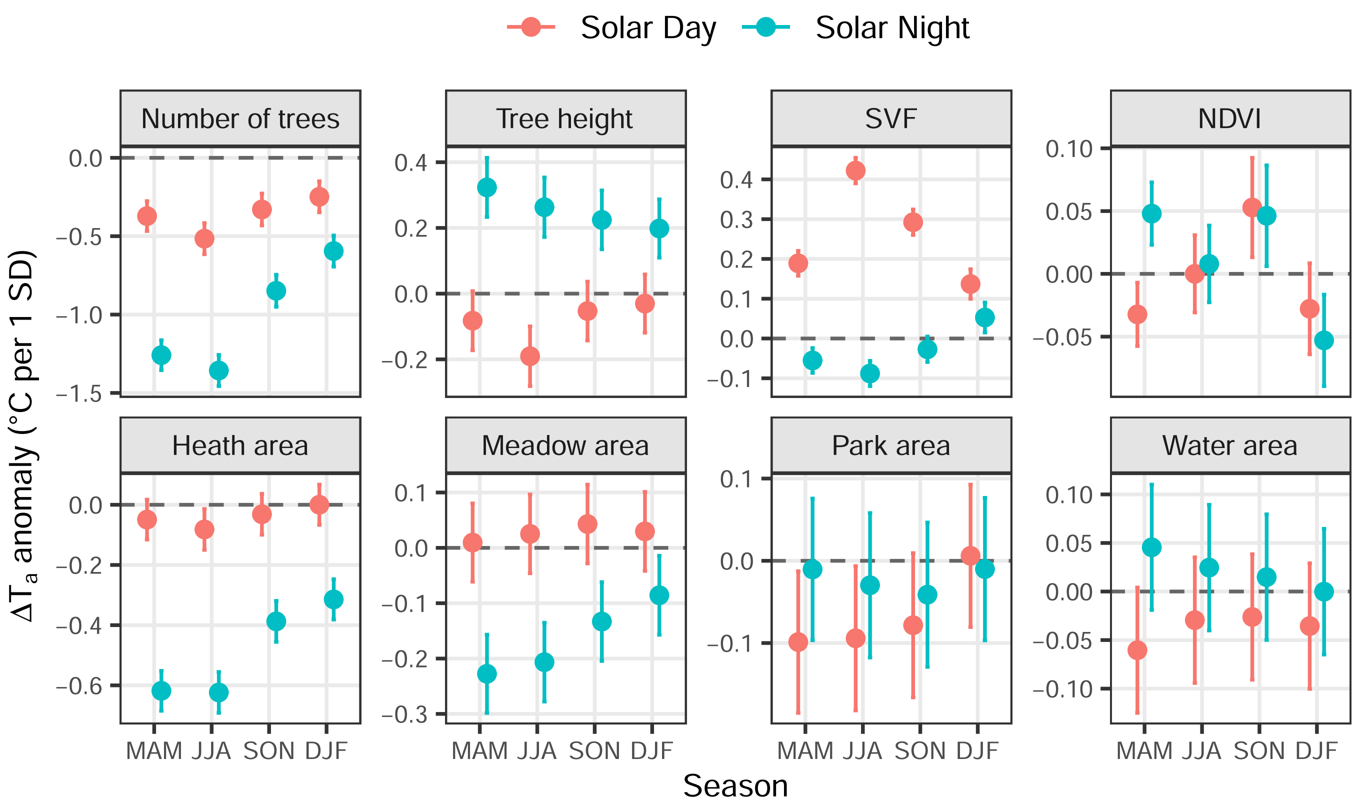

Fig. 8. Environmental drivers of T_a variability. Marginal trends (standardised effects per 1 SD change in the predictor) of environmental variables on daily T_a anomalies, estimated from the final LMM. Trends represent the change in T_a anomaly per 1-standard-deviation increase in the predictor and are shown separately for each season and solar period. Points indicate estimated marginal effects, with horizontal bars representing 95% confidence intervals.

indicated by the presence of a stable high-pressure system.

The logger measurements showed that the heatwave event developed progressively from 11 to 14 August 2024, with daily maximum T_a exhibiting an upward trend peaking on 13 August. However, the most demanding HTC conditions actually occurred one day earlier, as indicated by the derived thermal indices (Fig. 9b). mPET values were generally higher than UTCI values, exceeding 41 °C on 12 August, indicating very hot thermal sensations in R and H according to the PET range for Western and Central Europa (Matzarakis and Mayer, 1996). In comparison, the coolest sites (MF and BF) were more than 5 °C cooler, reducing the thermal sensation to hot (> 35 °C) or almost warm (< 35 °C). In general, R and UP were the warmest sites at night, with R experiencing a T_a anomaly of over + 4 °C between 11 and 12 August. During the day, the dense mixed forests (MF and BF) remained relatively cool, while the more open and sparsely covered H and PF sites became hotter than R at peak times.

When comparing T_a to UTCI and mPET patterns, a few things stand out. Firstly, the thermal indices indicate reduced differences between R and UP at night, likely because RH is consistently higher in UP than in R. Secondly, the relative differences between BF and MF are also reduced, especially during the day. This is probably because RH was lower in BF than in MF, and since BF had slightly lower SVF values (−0.08) on average than MF. Thirdly, while H and PF were warmer than R in terms of T_a at noon, this effect was substantially altered when considering heat indices, especially mPET. In fact, H and PF were not usually warmer than R, despite T_{MRT} being consistently highest in R. This discrepancy between T_a and the thermal indices highlights that HTC conditions are not solely determined by T_a. Although H and PF exhibited comparatively high daytime T_a values, their mPET and UTCI values remained lower than in the residential district. This likely reflects differences in radiative exposure, surface heat storage, and local moisture conditions associated with the contrasting vegetation structures and built environments. The results therefore suggest that open vegetated environments can still reduce physiological heat stress relative to built-up residential areas, even when daytime T_a alone indicates limited cooling.

4. Discussion

This study compares the microclimates of five structurally diverse UGS sites, revealing that microclimatic contrasts among UGS structures are shaped by vegetation and atmospheric conditions. The additional vegetated residential site allowed comparisons with the nearby urban park, while both sites allowed estimations of the cooling efficiency of vegetated and hybrid urban sites with more rural peri-urban forests. While the positive microclimatic effects of UGS (Aram et al., 2019) and trees (Rahman et al., 2020; Yang et al., 2025) are well documented, our study contributes to the existing literature by comparing microclimate regimes across different UGS structures under varying seasonal and synoptic forcings rather than focusing solely on absolute cooling magnitudes. The two-year observation period enabled a robust assessment of diurnal, seasonal, and synoptic influences.

Our results show that the study sites maintained distinct temperature regimes, while the magnitude of these contrasts varied systematically with time of day, season, and prevailing weather conditions. Temperature contrasts were generally more pronounced at night, intensified under warm conditions, and reached their greatest magnitudes during hot weather. Seasonal variability primarily modulated the strength of these contrasts, whereas the relative ranking of sites remained comparatively stable, particularly at night. During the summer months (JJA), dense peri-urban mixed forests provided the strongest daytime cooling, with the largest differences occurring during morning and afternoon hours. These sites also exhibited the smallest diurnal temperature variability throughout the year and were typically the coolest environments during the daytime. At night, however, sparsely vegetated

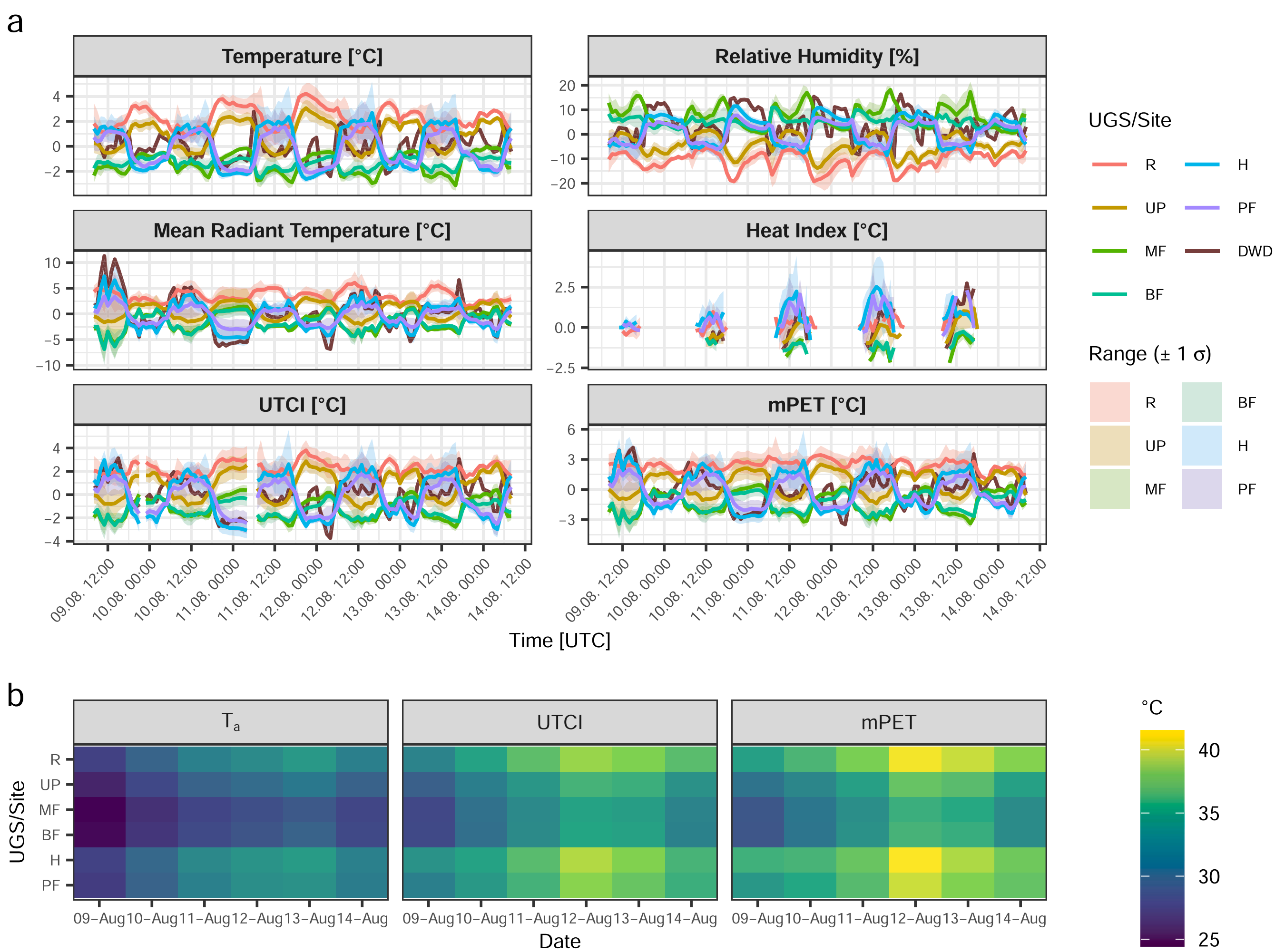

Fig 9. Heatwave event in August 2024. Time series of T_a, RH, T_{MRT}, HI, UTCI, and mPET anomalies before and during the HW event from August 2024 for all UGS structures/study sites, including the DWD reference. Shaded areas in all panels indicate one standard deviation across the T_a anomalies of the individual UGS loggers. HI was only defined when $T_a > 26.7$ °C and RH > 40%. UTCI calculation was only feasible for wind speeds between 0.341 and 11.568 m·s^{-1}. Anomalies were calculated relative to the mean T_a across the six study sites, excluding the DWD reference station (a). T_a, UTCI, and mPET heatmaps for the heatwave event in August 2024. The tiles show the maximum values for each day.

UGS emerged as the coolest sites, particularly during spring and summer. This contrasting day–night behaviour likely reflects the balance between daytime shading effects in dense canopies and enhanced nocturnal radiative cooling over more open vegetated surfaces with higher SVF (Zhao et al., 2023). Dense canopies may reduce nighttime heat loss through radiative trapping, whereas open sites retain a greater radiative cooling potential.

These findings are consistent with previous research on UGS microclimates. A systematic review by Bowler et al. (2010) highlighted the substantial cooling potential of urban vegetation compared with built environments. (Kirschner et al., 2023) found that compact UGSs of medium size (10–25 ha) with dense tree cover were the most effective at cooling the surrounding urban area. Similarly, Ren et al. (2018) showed that urban forests generate cool islands that are particularly pronounced during the warm season and depend strongly on structural vegetation attributes such as crown closure and leaf area index. Using modelling approaches, Meili et al. (2021) demonstrated that trees in Zurich provide the strongest cooling effects during the warm season, with maximum impacts in the afternoon and early evening. Seasonal contrasts comparable to our observations were also reported by Hamada and Ohta (2010), who found larger temperature differences between green areas and surrounding urban surfaces during summer and smaller contrasts during winter.

The modelling results further indicate that structural characteristics represented by tree number, tree height, and SVF are consistently associated with temperature anomalies. Tree density emerged as the strongest predictor of lower temperatures, particularly during spring and summer nights, whereas greater tree height was generally associated with slightly higher temperatures. These results broadly align with the meta-analysis by Rahman et al. (2020), which emphasised the importance of canopy density for urban cooling and recommended planting smaller trees with dense canopies for better shading. However, it should be noted that the cooling efficacy of trees can be influenced non-linearly by meteorological conditions such as temperature, humidity, and wind speed (Cheng et al., 2022; Su et al., 2022). Linear mixed-effects models assume constant responses within factor levels and may therefore mask threshold-driven processes, such as stomatal closure during hot, dry conditions. Additional environmental variables, such as above-ground biomass density, tree species composition, and detailed canopy metrics, were available only for the UFA sites and could further refine future modelling approaches.

As a main novelty, the present study explicitly integrates large-scale circulation types and demonstrates that the cooling performance of UGS is not constant but strongly modulated by the synoptic situation. Temperature contrasts increased under anticyclonic weather conditions and during warm weather, and decreased under cyclonic conditions, which are characterised by increased cloudiness and wind. While many classification approaches exist (Huth et al., 2008), the GWT classification scheme developed by Beck et al. (2007, 2015) was applied due to its intuitive interpretation and its suitability for regional climatological analyses. Our results are consistent with those of Zak et al. (2020), who used the GWT classification scheme to study nighttime UHI intensities in Prague and Bucharest. They found higher intensities under anticyclonic conditions with southerly winds in both cities. Contrary, the lowest intensities in Prague were observed under cyclonic northern types. Our results further support and extend the findings of Beck et al. (2018), who showed that undisturbed synoptic conditions lead to stronger T_a contrasts across LCZs in Augsburg, whereas increasing cloudiness and wind speed reduce these contrasts. In this context, the use of circulation-based weather types provides a more systematic framework for linking local microclimate variability to the large-scale atmospheric state. As studies found an increasing frequency and duration of persistent anticyclonic conditions in parts of Europe in recent decades (Tong et al., 2026) and for future climate projections (Jacobeit et al., 2017; Riediger and Gratzki, 2014), the amplification of microclimatic contrasts may become increasingly relevant for urban climate adaptation.

Improving outdoor HTC conditions is a key objective of climate-sensitive urban design (Ahmed et al., 2024). A recent review of 182 studies across 17 climates reported that urban trees can reduce UTCI by up to −6 °C, with most studies documenting reductions of −4 °C to −2 °C and PET reductions of −8 °C to −4 °C (Li et al., 2024). While many studies evaluate the cooling potential of trees within different urban morphologies (Kirschner et al., 2023; Li et al., 2024; Unger et al., 2018), our heatwave case illustrates how structural differences among UGS translate into measurable reductions in thermal stress under extreme conditions. Although the relative ranking of the sites remained stable, dense mixed forests (LCZ A) reduced maximum mPET by approximately −6 °C and UTCI by about −4.5 °C compared to the residential site (LCZ 5) during hot conditions ($T_a > 30$ °C). These reductions are consistent with the above documented ranges in the literature. Using a combination of measurements and proxy data, Unger et al. (2018) analysed HTC conditions across LCZs in Szeged during a 2015 heatwave and found maximum PET values exceeding 45 °C but relatively small intra-urban contrasts (−2.6 °C between LCZ 2 and LCZ D). The larger contrasts observed in our study likely reflect bigger structural differences between sites, lower heatwave intensity, or methodological differences between PET and mPET calculations. Overall, the heatwave therefore acted as a natural experiment demonstrating that dense peri-urban forests maintain a substantial heat-stress mitigation potential even under extreme atmospheric forcing, whereas sparsely vegetated sites provide only limited reductions.

While our findings highlight robust structural patterns, their transferability depends on the representativeness of UGS structures and background climate, as well as on the validity of climate measurements. The measurement data were collected by over thirty MX2301A HOBO loggers from Onset (Onset, 2022) placed inside identical 3D-printed radiation shields. Although the sensitivity tests (see supplementary material S2.4.1) suggest that T_a was overestimated during the daytime (+1.42 °C), particularly around midday under clear-sky conditions, compared to custom-made shields, it is reasonable to assume that this bias is consistent across all logger sites. Furthermore, T_a values from five to seven loggers within each study site were averaged ensuring more robust data. The two-year observation period showed good agreement with the 30-year climatological normal in both local meteorological conditions and large-scale weather types, suggesting that the observed microclimatic patterns are not atypical. Our results can likely be transferred to structurally similar peri-urban forests and urban parks in temperate climates. However, the study remains local in scale and focuses on a limited number of UGS structures within a specific urban–rural setting. Consequently, the absolute magnitude of the observed temperature contrasts and the relative importance of individual predictors may differ in other climatic or urban contexts. Nevertheless, the identified relationships between vegetation structure, atmospheric conditions, and microclimatic variability are consistent with established physical processes and previous findings from urban climate research. One potential exception is the heathland site, whose elongated and comparatively narrow spatial configuration may promote stronger exchange with adjacent environments and thus limit the development of an isolated heathland microclimate. The site may therefore function more as a vegetated corridor than as a compact patch. Consequently, the observed temperature magnitudes should be interpreted with caution and may not be fully transferable to larger or more spatially continuous heathland systems. Nevertheless, the underlying microclimatic processes observed at the site – particularly strong radiative cooling associated with sparse tree cover and high sky exposure – are likely characteristic of open heathland environments more generally. Furthermore, each UGS structure was represented by a single study site. The observed patterns should therefore not be interpreted as universally representative for all mixed forests, pine forests, heathlands, or urban parks. Instead, the study identifies process-based relationships between vegetation structure, atmospheric conditions, and microclimatic variability within representative local examples of these UGS structures. However, the comparatively small number of intensively monitored sites enabled continuous long-term observations over two complete annual cycles, providing a level of temporal robustness that is often lacking in short-term intensive observation campaigns.

From an urban-planning perspective, the results emphasise the importance of structurally complex vegetation for heat-stress mitigation (Arzberger et al., 2025). Dense peri-urban forests showed the strongest cooling potential, whereas sparsely vegetated sites provided only limited thermal relief during hot conditions. In the UFA, pine forests are currently characterised by low canopy density and declining tree health (Ritter et al., 2025), which likely reduces their cooling efficiency relative to nearby mixed forests. Ongoing reforestation strategies that aim to increase structural diversity and reduce the dominance of pine to around 40% therefore align well with the microclimatic benefits identified in this study (Stadt Augsburg, 2026). In general, increasing structural vegetation complexity and promoting mixed forest stands may enhance both climate resilience and microclimatic cooling in peri-urban landscapes. Reforestation efforts should thereby prioritise tree species that can cope with the warming expected for Southern Bavaria, such as *Abies alba*, *Fagus sylvatica*, *Fraxinus excelsior*, and *Quercus robur* (Dyderski et al., 2018). Despite their lower cooling performance, UGS with lower structural vegetation complexity, such as heathlands, may still provide important ecological and recreational benefits (Rathmann et al., 2022).

To further study associations among UGS microclimates, health effects, and subjective perceptions of different UGS structures, we invited participants to engage in climate walks at some of the UGS sites and the residential site studied here. We investigated bioclimatic variability along the routes, measured heart rates and cortisol levels, and interviewed people about their subjective perceptions during the walks. While some publications are still being prepared, the first results have been published by Can et al. (2025) and Mahesh et al. (2023, 2025), demonstrating physiological, psychological, and cognitive responses to walking in natural and built urban environments. This study approximated HTC conditions based on nearby official DWD measurements. During the climate walks, T_a, RH, wind speed, and globe temperature were directly recorded, hence allowing a more precise and spatially explicit approximation of thermal indices such as UTCI. Mobile and long-term climate measurements form the basis for validating numerical UGS microclimate models with ENVI-met (Bruse and Fleer, 1998), as recently implemented by Simon et al. (2026). The modelling perspective further enables comparisons of UGS microclimates under different meteorological forcings (heat days, clear-sky conditions, dry soils, climate change) and the bioclimatic evaluation of various silvicultural scenarios (reforestation, forest conversion). It also provides an opportunity to add blue elements into UGS and thus study the synergistic effects of green and blue infrastructures (Gunawardena et al., 2017).

Funding sources

This work was supported by the German Research Foundation (DFG) under grant number 471909988.

CRediT authorship contribution statement

Jonathan Simon: Writing – review & editing, Writing – original draft, Visualization, Validation, Supervision, Software, Methodology, Investigation, Formal analysis, Data curation, Conceptualization. **Max Stocker:** Validation, Software, Data curation. **Lisa-Marie Falkenrodt:** Data curation. **Bhargavi Mahesh:** Writing – review & editing. **Joachim Rathmann:** Writing – review & editing, Funding acquisition. **Wolfgang Buermann:** Writing – review & editing. **Yekta Said Can:** Resources. **Elisabeth André:** Writing – review & editing, Supervision, Funding acquisition. **Christoph Beck:** Writing – review & editing, Supervision, Resources, Project administration, Funding acquisition, Conceptualization.

Declaration of Generative AI and AI-assisted technologies in the writing process

During the preparation of this work, the authors used DeepL Write, Grammarly, and ChatGPT to improve the language of the manuscript. After using these tools, the authors reviewed and edited the content as needed and take full responsibility for the content of the published article.

Declaration of Competing Interest

The authors declare that they have no known competing financial interests or personal relationships that could have appeared to influence the work reported in this paper.

Acknowledgements

We would like to thank the Augsburg Forestry Administration, the Augsburg City Council and the Landscape Conservation Association for allowing us to mount our measuring devices to trees and lampposts.

Appendix A. Supporting information

Supplementary data associated with this article can be found in the online version at doi:10.1016/j.ufug.2026.129617.

References

Adams, R.E., Lee, C.C., Smith, E.T., Sheridan, S.C., 2021. The relationship between atmospheric circulation patterns and extreme temperature events in North America. Int. J. Climatol. 41 (1), 92–103. https://doi.org/10.1002/joc.6610.

Ahmed, N.M., Altamura, P., Giampaoletti, M., Hemeida, F.A., Mohamed, A.F.A., 2024. Optimizing human thermal comfort and mitigating the urban heat island effect on public open spaces in Rome, Italy through sustainable design strategies. Sci. Rep. 14 (1), 19931. https://doi.org/10.1038/s41598-024-65794-8.

Aram, F., García, E.H., Solgi, E., Mansournia, S., 2019. Urban green space cooling effect in cities. Heliyon 5 (4). https://doi.org/10.1016/j.heliyon.2019.e01339.

Arzberger, S., Brunschweiger, B., Egerer, M., Suda, M., Thom, D., Annighöfer, P., 2025. Small but powerful? The seasonal and diurnal cooling potential of urban green spaces in Munich, Germany, is moderated by size and vegetation complexity. Urban. For. & Urban. Green. 112, 128934. https://doi.org/10.1016/j.ufug.2025.128934.

Beck, C., Jacobeit, J., Jones, P.D., 2007. Frequency and within-type variations of large-scale circulation types and their effects on low-frequency climate variability in central europe since 1780. Int. J. Climatol. 27 (4), 473–491. https://doi.org/10.1002/joc.1410.

Beck, C., Philipp, A., Jacobeit, J., 2015. Interannual drought index variations in Central Europe related to the large-scale atmospheric circulation—Application and evaluation of statistical downscaling approaches based on circulation type classifications. Theor. Appl. Climatol. 121 (3–4), 713–732. https://doi.org/10.1007/s00704-014-1267-z.

Beck, C., Straub, A., Breitner, S., Cyrys, J., Philipp, A., Rathmann, J., Schneider, A., Wolf, K., Jacobeit, J., 2018. Air temperature characteristics of local climate zones in the Augsburg urban area (Bavaria, southern Germany) under varying synoptic conditions. Urban. Clim. 25, 152–166. https://doi.org/10.1016/j.uclim.2018.04.007.

Bowler, D.E., Buyung-Ali, L., Knight, T.M., Pullin, A.S., 2010. Urban greening to cool towns and cities: a systematic review of the empirical evidence. Landsc. Urban. Plan. 97 (3), 147–155. https://doi.org/10.1016/j.landurbplan.2010.05.006.

Brandt, L., Derby Lewis, A., Fahey, R., Scott, L., Darling, L., Swanston, C., 2016. A framework for adapting urban forests to climate change. Environ. Sci. & Policy 66, 393–402. https://doi.org/10.1016/j.envsci.2016.06.005.

Bröde, P., Fiala, D., Błażejczyk, K., Holmér, I., Jendritzky, G., Kampmann, B., Havenith, G., 2012. Deriving the operational procedure for the Universal Thermal Climate Index (UTCI). Int. J. Biometeorol. 56 (3), 481–494.

Bruse, M., Fleer, H., 1998. Simulating surface–plant–air interactions inside urban environments with a three dimensional numerical model. Environ. Model. Softw. 13 (3–4), 373–384.

Can, Y.S., Rathmann, J., Beck, C., Mahesh, B., Simon, J., Stocker, M., Falkenrodt, L.-M., Brandl, S., André, E., 2025. EEG-based differentiation of forest and urban walking environments using machine learning. 47th Annu. Int. Conf. IEEE Eng. Med. Biol. Soc. (EMBC) 2025, 1–6. https://doi.org/10.1109/EMBC58623.2025.11253034.

Cea, L., Costabile, P., 2022. Flood risk in urban areas: Modelling, management and adaptation to climate change. A review. Hydrology 9 (3), 50.

Chen, Y.-C., 2023. Thermal indices for human biometeorology based on Python. Sci. Rep. 13 (1), 20825. https://doi.org/10.1038/s41598-023-47388-y.

Chen, Y.C., Matzarakis, A., 2018. Modified physiologically equivalent temperature—basics and applications for western European climate. Theor. Appl. Climatol. 132 (3), 1275–1289.

Cheng, X., Peng, J., Dong, J., Liu, Y., Wang, Y., 2022. Non-linear effects of meteorological variables on cooling efficiency of African urban trees. Environ. Int. 169, 107489. https://doi.org/10.1016/j.envint.2022.107489.

Christen, A., Vogt, R., 2004. Energy and radiation balance of a central European city. Int. J. Climatol. 24 (11), 1395–1421. https://doi.org/10.1002/joc.1074.

Dodman, D., Hayward, B., Pelling, M., Castan Broto, V., Chow, W., Chu, E., Dawson, R., Khirfan, L., McPhearson, T., Prakash, A., Zheng, Y., Ziervogel, G., 2022. Cities, Settlements and Key Infrastructure. In: Roberts, D.C., Tignor, M., Poloczanska, E.S., Mintenbeck, K., Alegría, A., Craig, M., Langsdorf, S., Löschke, S., Möller, V., Okem, A., Rama, B. (Eds.), Climate Change 2022: Impacts, Adaptation and Vulnerability, Contribution of Working Group II to the Sixth Assessment Report of the Intergovernmental Panel on Climate Change. Cambridge University Press, Cambridge, UK and New York, NY, USA, pp. 907–1040. https://doi.org/10.1017/9781009325844.008 [H.-O. Pörtner.

DWD, 2026. Deutscher Wetterdienst. Data downloaded from the Open Data server at https://opendata.dwd.de (last accessed: 2026-08-06). Licence: CC BY 4.0: https://creativecommons.org/licenses/by/4.0/.

Dyderski, M.K., Paź, S., Frelich, L.E., Jagodziński, A.M., 2018. How much does climate change threaten European forest tree species distributions? Glob. Change Biol. 24 (3), 1150–1163. https://doi.org/10.1111/gcb.13925.

Elmqvist, T., Fragkias, M., Goodness, J., Güneralp, B., Marcotullio, P.J., McDonald, R.I., Parnell, S., Schewenius, M., Sendstad, M., Seto, K.C., & Wilkinson, C. (Eds). (2013). Urbanization, Biodiversity and Ecosystem Services: Challenges and Opportunities: A Global Assessment. Springer Netherlands. https://doi.org/10.1007/978-94-007-7088-1.

Founda, D., Santamouris, M., 2017. Synergies between Urban Heat Island and Heat Waves in Athens (Greece), during an extremely hot summer (2012). Sci. Rep. 7 (1), 10973. https://doi.org/10.1038/s41598-017-11407-6.

German, Aerospace Center, 2019. Sentinel-2 MSI - Level 3A (MAJA/WASP Tiles)—Germany [Data set]. Ger. Aerosp. Cent. (DLR). https://doi.org/10.15489/4HCQ6DGKJ648.

Gunawardena, K.R., Wells, M.J., Kershaw, T., 2017. Utilising green and bluespace to mitigate urban heat island intensity, 1040–1055 Sci. Total. Environ. *584–585*. https://doi.org/10.1016/j.scitotenv.2017.01.158.

Hamada, S., Ohta, T., 2010. Seasonal variations in the cooling effect of urban green areas on surrounding urban areas. Urban. For. & Urban. Green. 9 (1), 15–24. https://doi.org/10.1016/j.ufug.2009.10.002.

Hersbach, H., Bell, B., Berrisford, P., Biavati, G., Horányi, A., Muñoz Sabater, J., Nicolas, J., Peubey, C., Radu, R., Rozum, I., Schepers, D., Simmons, A., Soci, C., Dee, D., Thépaut, J.-N., 2023. *ERA5 hourly data on single levels from 1940 to present.* Copernic. Clim. Change Serv. (C3S) Clim. Data Store (CDS) [Data Set.]. https://doi.org/10.24381/cds.adbb2d47.

Hess, P., Brezowsky, H., 1969. Katalog der grosswetterlagen Europas, 15. Deutscher Wetterdienst, Offenbach am Main, Germany.

Hondula, D.M., Vanos, J.K., Gosling, S.N., 2014. The SSC: a decade of climate–health research and future directions. Int. J. Biometeorol. 58 (2), 109–120. https://doi.org/10.1007/s00484-012-0619-6.

Huth, R., Beck, C., Philipp, A., Demuzere, M., Ustrnul, Z., Cahynová, M., Kyselý, J., Tveito, O.E., 2008. Classifications of atmospheric circulation patterns. Ann. New. Y. Acad. Sci. 1146 (1), 105–152. https://doi.org/10.1196/annals.1446.019.

Jacobeit, J., Homann, M., Philipp, A., Beck, C., 2017. Atmospheric circulation types and extreme areal precipitation in southern central Europe. Adv. Sci. Res. 14, 71–75. https://doi.org/10.5194/asr-14-71-2017.

Kirschner, V., Macků, K., Moravec, D., Maňas, J., 2023. Measuring the relationships between various urban green spaces and local climate zones. Sci. Rep. 13 (1), 9799. https://doi.org/10.1038/s41598-023-36850-6.

LDBV, 2024. Bayerische Vermessungsverwaltung – www.geodaten.bayern.de (last accessed: 2028-08-06). Licence: CC BY 4.0: https://creativecommons.org/licenses/by/4.0/. Data processed for research.

Li, D., Bou-Zeid, E., 2013. Synergistic interactions between urban heat islands and heat waves: the impact in cities is larger than the sum of its parts. J. Appl. Meteorol. Climatol. 52 (9), 2051–2064. https://doi.org/10.1175/JAMC-D-13-02.1.
Li, H., Zhao, Y., Wang, C., Ürge-Vorsatz, D., Carmeliet, J., Bardhan, R., 2024. Cooling efficacy of trees across cities is determined by background climate, urban morphology, and tree trait. Commun. Earth & Environ. 5 (1), 754. https://doi.org/10.1038/s43247-024-01908-4.
Lindberg, F., Holmer, B., 2024, August 14. Sky View Factor Calculator. User Manual—Version 1.1. Göteborg Urban Climate Group, Department of Earth Sciences. University of Gothenburg.
Mahesh, B., Nasir, J., Klein, S., Hallmen, T., Can, Y., Simon, J., Beck, C., Rathmann, J., Stocker, M., Falkenrodt, L.-M., Andre, E., 2025, September 24. Physiological and cognitive responses to walking in natural and built urban environments. IEEE-EMBS Int. Conf. Body Sens. Netw. 2025. https://openreview.net/forum?id=4ufxj1sKUm.
Mahesh, B., Seiderer, A., Dietz, M., André, E., Simon, J., Rathmann, J., Beck, C., Can, Y. S., 2023. Investigating psychological and physiological effects of forest walking: a machine learning approach. 11th Int. Conf. Affect. Comput. Intell. Interact. Workshops Demos (ACIIW) 2023, 1–8. https://doi.org/10.1109/ACIIW59127.2023.10388180.
Matzarakis, A., Mayer, H., 1996. Another kind of environmental stress: thermal stress. WHO Newsl. 18, 7–10.
Matzarakis, A., Rutz, F., Mayer, H., 2007. Modelling radiation fluxes in simple and complex environments—Application of the RayMan model. Int. J. Biometeorol. 51 (4), 323–334. https://doi.org/10.1007/s00484-006-0061-8.
Matzarakis, A., Rutz, F., Mayer, H., 2010. Modelling radiation fluxes in simple and complex environments: Basics of the RayMan model. Int. J. Biometeorol. 54 (2), 131–139. https://doi.org/10.1007/s00484-009-0261-0.
Meili, N., Manoli, G., Burlando, P., Carmeliet, J., Chow, W.T.L., Coutts, A.M., Roth, M., Velasco, E., Vivoni, E.R., Fatichi, S., 2021. Tree effects on urban microclimate: Diurnal, seasonal, and climatic temperature differences explained by separating radiation, evapotranspiration, and roughness effects. Urban. For. & Urban. Green. 58, 126970. https://doi.org/10.1016/j.ufug.2020.126970.
Oke, T.R., Mills, G., Christen, A., Voogt, J.A., 2017. Urban Climates. Cambridge University Press.
Oliveira, A., Lopes, A., Correia, E., Niza, S., Soares, A., 2021. An urban climate-based empirical model to predict present and future patterns of the Urban Thermal Signal. Sci. Total. Environ. 790, 147710. https://doi.org/10.1016/j.scitotenv.2021.147710.
Onset, *2020. Pro v2 Data Logger (U23-00x) User's Manual | Onset's HOBO Data Loggers*. https://www.onsetcomp.com/sites/default/files/resources-documents/10694-Q%20U23%20Manual.pdf (last accessed: 2026-08-06).
Onset, 2022. HOBO® MX2300 Series Data Logger Manual | Onset's HOBO Data Loggers. https://www.onsetcomp.com/sites/default/files/2023-01/20923-O%20MX2300%20Manual.pdf (last accessed: 2026-08-06).
OpenStreetMap, *2024*. https://www.openstreetmap.de/. Data is available under the Open Database License: https://www.openstreetmap.org/copyright.
Perkins-Kirkpatrick, S.E., Lewis, S.C., 2020. Increasing trends in regional heatwaves. Nat. Commun. 11 (1), 3357. https://doi.org/10.1038/s41467-020-16970-7.
Philipp, A., Bartholy, J., Beck, C., Erpicum, M., Esteban, P., Fettweis, X., Huth, R., James, P., Jourdain, S., Kreienkamp, F., Krennert, T., Lykoudis, S., Michalides, S.C., Pianko-Kluczynska, K., Post, P., Álvarez, D.R., Schiemann, R., Spekat, A., Tymvios, F. S., 2010. Cost733cat – A database of weather and circulation type classifications. *Physics and Chemistry of the Earth, Parts A/B/C*. Classif. Atmos. Circ. Patterns Theory Appl. 35 (9), 360–373. https://doi.org/10.1016/j.pce.2009.12.010.
Pinheiro, J., Bates, D., Saikat, D., Sarkar, D., EISPACK, authors, Heisterkamp, S., Van Willigen, B., Ranke, J., R Core Team, 2025. nlme Linear Nonlinear Mixed Eff. Models 3.1–168. https://doi.org/10.32614/CRAN.package.nlme ([Data set]).
R Core Team, 2024. *R: A Language and Environment for Statistical Computing.* (Version 4.4.2) [Computer software]. R. Found. Stat. Comput. Vienna Austria. https://www.R-project.org.
Rahman, M.A., Stratopoulos, L.M.F., Moser-Reischl, A., Zölch, T., Häberle, K.-H., Rötzer, T., Pretzsch, H., Pauleit, S., 2020. Traits of trees for cooling urban heat islands: a meta-analysis. Build. Environ. 170, 106606. https://doi.org/10.1016/j.buildenv.2019.106606.
Rathmann, J., Korpela, K.M., Stojakowits, P., 2022. Pleistocene hypothesis – moving savanna perceptual preference hypothesis beyond Savanna. Front. Psychol. 13. https://doi.org/10.3389/fpsyg.2022.901799.
Ren, Z., He, X., Pu, R., Zheng, H., 2018. The impact of urban forest structure and its spatial location on urban cool island intensity. Urban. Ecosyst. 21 (5), 863–874. https://doi.org/10.1007/s11252-018-0776-4.
Riediger, U., Gratzki, A., 2014. Future weather types and their influence on mean and extreme climate indices for precipitation and temperature in Central Europe. Meteorol. Z. 23 (3), 231–252. https://doi.org/10.1127/0941-2948/2014/0519.
Ritter, S., Burgdorf, N., Hahn, A., 2025: Kiefernvitalität nach Hagelschlag: Womit die Kiefer im Augsburger Lechauwald zu kämpfen hat. https://www.waldwissen.net/de/waldwirtschaft/schadensmanagement/komplexkrankheiten/kiefernvitalitaet-nach-hagelschlag (last accessed: 2026-08-06).
Sicard, P., Agathokleous, E., Anenberg, S.C., De Marco, A., Paoletti, E., Calatayud, V., 2023. Trends in urban air pollution over the last two decades: A global perspective. Sci. Total Environ. 858, 160064.
Simon, J., Ertl, M., Naumann, M., Braadt, L., Hammel, G., Philipp, A., Jacobeit, J., Beck, C., 2024. The influence of specific weather types on stroke occurrence: An analysis of 23,000 patients from Augsburg, Germany. Int. J. Environ. Health Res. 0 (0), 1–12. https://doi.org/10.1080/09603123.2024.2404474.
Simon, J., Oster, J., Beck, C., 2026. Impact of tree representation on urban climate modelling: Insights from ENVI-met simulations in Augsburg, Germany. Urban. Clim. 67, 102879. https://doi.org/10.1016/j.uclim.2026.102879.
Stadt Augsburg, 2026. Lichte Kiefernwälder: Neues Konzept zum Erhalt. https://www.augsburg.de/umwelt-soziales/umwelt/stadtwald/waldschutzprogramm (last accessed: 2026-08-06).
Stewart, I.D., Oke, T.R., 2012. Local climate zones for urban temperature studies. Bull. Am. Meteorol. Soc. 93 (12), 1879–1900. https://doi.org/10.1175/BAMS-D-11-00019.1.
Su, Y., Wu, J., Zhang, C., Wu, X., Li, Q., Liu, L., Bi, C., Zhang, H., Lafortezza, R., Chen, X., 2022. Estimating the cooling effect magnitude of urban vegetation in different climate zones using multi-source remote sensing. Urban. Clim. 43, 101155. https://doi.org/10.1016/j.uclim.2022.101155.
Tong, Y., Sun, C., Lou, W., Dong, M., Shi, L., Song, Z., He, Y., 2026. Changes in persistent anticyclonic circulation across Eurasian continent and its linkage with extreme heatwaves. Glob. Planet. Change 256, 105183. https://doi.org/10.1016/j.gloplacha.2025.105183.
Ulgiati, S., Zucaro, A., 2019. Challenges in urban metabolism: sustainability and well-being in cities. Front. Sustain. Cities 1. https://doi.org/10.3389/frsc.2019.00001.
Unger, J., Skarbit, N., Gál, T., 2018. Evaluation of outdoor human thermal sensation of local climate zones based on long-term database. Int. J. Biometeorol. 62 (2), 183–193. https://doi.org/10.1007/s00484-017-1440-z.
Veerkamp, C.J., Schipper, A.M., Hedlund, K., Lazarova, T., Nordin, A., Hanson, H.I., 2021. A review of studies assessing ecosystem services provided by urban green and blue infrastructure. Ecosyst. Serv. 52, 101367. https://doi.org/10.1016/j.ecoser.2021.101367.
Verdonck, M.-L., Demuzere, M., Hooyberghs, H., Beck, C., Cyrys, J., Schneider, A., Dewulf, R., Van Coillie, F., 2018. The potential of local climate zones maps as a heat stress assessment tool, supported by simulated air temperature data. Landsc. Urban. Plan. 178, 183–197. https://doi.org/10.1016/j.landurbplan.2018.06.004.
Wickham, H., Averick, M., Bryan, J., Chang, W., McGowan, L.D., François, R., Grolemund, G., Hayes, A., Henry, L., Hester, J., Kuhn, M., Pedersen, T.L., Miller, E., Bache, S.M., Müller, K., Ooms, J., Robinson, D., Seidel, D.P., Spinu, V., Yutani, H., 2019. Welcome to the Tidyverse. J. Open. Source Softw. 4 (43), 1686. https://doi.org/10.21105/joss.01686.
Yang, X., Li, B., Li, N., Ma, X., 2025. A study of the cooling effect of urban trees: Influencing factors, assessment methods, planning strategies, and impacts. Theor. Appl. Climatol. 157 (1), 31. https://doi.org/10.1007/s00704-025-05904-2.
Yarnal, B., 1993. Synop. Climatol. Environ. Anal.
Zak, M., Nita, I.-A., Dumitrescu, A., Cheval, S., 2020. Influence of synoptic scale atmospheric circulation on the development of urban heat island in Prague and Bucharest. Urban. Clim. 34, 100681. https://doi.org/10.1016/j.uclim.2020.100681.
Zhao, Y., Li, H., Bardhan, R., Kubilay, A., Li, Q., Carmeliet, J., 2023. The time-evolving impact of tree size on nighttime street canyon microclimate: wind tunnel modeling of aerodynamic effects and heat removal. Urban. Clim. 49, 101528. https://doi.org/10.1016/j.uclim.2023.101528.
Zuur, A.F., Ieno, E.N., Walker, N., Saveliev, A.A., Smith, G.M., 2009. Mixed effects models and extensions in ecology with R. Springer. https://doi.org/10.1007/978-0-387-87458-6.